Non-destructive characterisation of N/Al level in P91 steels using electromagnetic sensors

J. Liu, M. Strangwood, C. L. Davis & J. Parker

Non-destructive characterisation of N/Al level in P91 steels using electromagnetic sensors

J. Liu*[1], M. Strangwood[1], C. L. Davis[1] and J. Parker[2]

P91 steels with different N/Al ratios short term tempered or long term aged at a series of temperatures have been characterised using a multifrequency electromagnetic sensor. It was found that the low frequency inductance value is sensitive to the intralath MX precipitates that determine the mean free path for domain wall motion and hence the initial relative permeability of the steels. The electromagnetic sensor is capable of separating P91 steels with low N/Al ratio in the service entry or early service state. In contrast, the hardness measurements were found to be insensitive to the N/Al ratio for the short term tempered samples.

Keywords: N/Al ratio, P91 steel, MX precipitate, Electromagnetic sensor, Hardness

Introduction

Steels containing 9Cr–1Mo (wt-%) are commonly used in the construction of power plant because they have good creep strength at high temperatures. However, for service in ultrasupercritical scenarios, it is necessary to modify the chemical composition with additions of niobium and vanadium in order to form carbonitrides that further enhance the creep strength[1–3] as well as toughness.[4] Such an alloy is often known as modified 9Cr1Mo or more commonly P91 steel. The carbonitrides, predominantly (Nb, V) (C, N) and often referred to as MX, where M denotes Nb and/or V and X denotes C and/or N, mostly form within the martensitic laths during tempering.[5,6] The availability of free nitrogen is critical to the precipitation of MX in P91 steels and can be affected by the presence of other nitride forming elements, e.g. Al. AlN precipitates can form during the manufacturing process of the steel plate and are not redissolved by the subsequent normalising and tempering heat treatments. The formation of AlN, and therefore the depletion of free nitrogen, significantly reduces the number density of MX precipitates and hence degrades the resistance to tempering and creep.[7,8] These effects can result in microstructural degradation with an associated loss of strength and, in the extreme, early failure of P91 steel components.[9] For example, it was reported that, in 2004, extensive type IV cracking had been found on branch and attachment welds on a P91 header after 58 000 h of service in a power plant, and the low N/Al ratio components were identified as a factor to this premature failure.[8] Therefore, the N/Al ratio in P91 steels is important to their MX precipitation, and a minimum value of this ratio is recommended by the Electric Power Research Institute (EPRI)[10] to be 4·0. It is desirable for the power industries and steel manufacturers to be able to non-destructively examine and distinguish P91 steel components that exhibit degraded microstructures before they enter service to avoid early failure. However, the conventional inspection techniques currently used by the power generation industries, such as examination of surface replicas or hardness measurements, are only suitable for application to limited spot checks. Moreover, these methods are not able to characterise the fine MX precipitates due to the limited resolution of the surface replica technique[11] or lack of specificity to fine microstructural detail for hardness measurement. Thus, a more comprehensive approach to assessment of the microstructure in P91 would be of significant benefit.

Among a wide range of non-destructive testing techniques available, electromagnetic (EM) methods are of particular interest for evaluation of ferromagnetic ferritic heat resistant steels such as P91 steels. Ferromagnetic materials such as ferritic steels contain magnetic domains, consisting of aligned magnetic moments, separated by domain walls. Each magnetic moment has associated with it a certain amount of free energy. The existence of domains is a consequence of energy minimisation. As magnetic field is applied, domains will be realigned through domain wall motion, domain nucleation and growth and/or domain rotation until a new minimum free energy state is reached. Microstructural features can interact with these processes to modify the energy balance and ease of domain realignment and hence affect the magnetic properties of ferromagnetic materials. More details on the domain theory and the effects of microstructure of ferromagnetic materials on their magnetic domains and properties can be found elsewhere.[12] Electromagnetic based sensors use applied magnetic fields with different magnitudes and directions and pick up the EM signals in a variety of forms depending on the type of the EM technique used and the nature of the domain movement. For example, irreversible domain wall motion past pinning features in a ferromagnetic material can be detected as a sharp

[1]School of Metallurgy and Materials, University of Birmingham, Edgbaston, Birmingham B15 2TT, UK
[2]Electrical Power Research Institute, 1300 West W.T. Harris Boulevard, Charlotte, NC 28262, USA

*Corresponding author, email sam.j.liu@gmail.com

pulse voltage in a search coil wound around the specimen, which is known as magnetic Barkhausen emission (MBE) or Barkhausen noise.[13] It has been reported that microstructural changes (e.g. precipitation during tempering or creep tests) result in changes in the magnetic properties of P91 steel.[14–16] Bong *et al.*[17] reported an EM sensor system for measuring the changes in the reversible magnetic permeability of a P91 steel isothermally aged at 690°C for different periods of time and assessed the remnant life of the steel by looking at the relationship between a magnetic parameter called peak interval of reversible magnetic permeability (about twice the coercivity force) and the Larson–Miller parameter (LMP). However, the reported peak interval of reversible magnetic permeability data were scattered and less sensitive than the mechanical properties such as yield strength and tensile strength to the LMP. Magnetic hysteresis loop (also known as *BH* loop) and MBE techniques have also been used to evaluate microstructural changes in P91 steels during creep tests under 125 MPa stress at 600°C (Refs. 14 and 15) or tempering at different temperatures (ranging from 650 to 950°C).[16] Changes in the normalised values of the measured coercivity and remanence, as opposed to the absolute values of these fundamental material properties independent of the sensor systems and/or sample geometry, or the MBE parameters such as the peak height/position of the root mean square of voltage profiles, were correlated qualitatively to microstructural changes (e.g. precipitation of large carbides or Laves phase),[14,15] mechanical hardness[16] or used to indicate different creep stage.[15] Moorthy *et al.*[18] reported correlation between the microstructural changes including grain/lath coarsening and precipitation and MBE parameters in a 9Cr–1Mo steel tempered at 650°C for different periods of time. A maximum MBE peak occurred at an intermediate tempering time (~10 h) when there was a certain combination of particle size distribution (affecting magnetic domain pinning strength) and interparticle spacing (affecting mean free path of the domain wall displacement). It should be noted that there is only empirical linkage between MBE parameters and materials magnetic properties, whereas relationships between EM sensor signals (e.g. mutual inductance) and relative permeability and resistivity can be mathematically described through classical EM theory. The relative permeability has been quantitatively related to the microstructure for certain steel structures,[19–21] and there are many relationships between resistivity and steel composition[22–24] and microstructure.[22,25,26] Although one can extract a variety of micromagnetic properties including coercivity, remanence, spontaneous magnetisation and differential permeability from a major *BH* loop, it is difficult to obtain a full major *BH* loop accurately on an open sample or a power plant component using a surface type probe as an encircling coil cannot be deployed for measuring the magnetic induction *B*; the sample geometry will influence the measured magnetic field *H* value due to geometric effects on both the internal and the external demagnetising fields. Moreover, it would be very difficult, if not impossible, to bring the whole sample/component to magnetic saturation. Thus, the measured signal would be composed of responses from the saturated and the unsaturated sections of the material, not to mention that

it would take a lot of power to magnetically saturate the part, which is obviously undesirable for field inspection/deployment, and it would be difficult to demagnetise the part; thus, the starting point of the measured *BH* loops for this or the next measurements would be uncertain. Therefore, the results from the samples of different dimensions (e.g. pipes/tubes of different diameter or wall thickness) are not directly comparable. By contrast, multifrequency EM sensor measurements are practically independent of sample geometry/dimensions as long as the sample area is sufficiently larger than the sensor to avoid edge effects, and the thickness is greater than the skin depth, which, in most cases, would not be an issue in the power generation industries.

Multifrequency EM sensors have proved sensitive to the change of ferrite/austenite fraction,[19,27] shown using model alloys, *in situ* analysis and finite element based modelling software. Prototype EM sensors are being used for *in situ* monitoring of the γ→α transformation during steel processing.[28] Electromagnetic sensors have also been used to detect decarburisation,[29,30] shown with high carbon steels for on- and offline monitoring. The theory as to how the relative permeability and resistivity of a sample affect the multifrequency EM response, for any sensor geometry, is presented elsewhere.[31] It has been shown that the multifrequency EM sensors are able to detect the initial relative permeability and resistivity changes, resulting from microstructural changes in P9 and T22 power plant steels during service at high temperatures.[32]
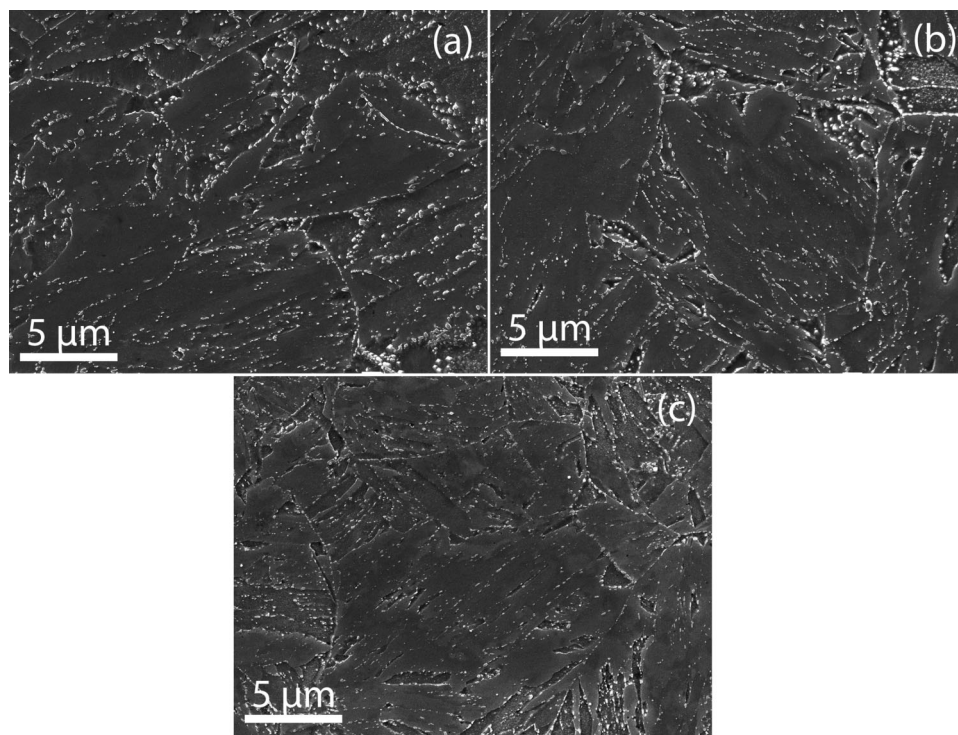
Although there has been significant work on magnetic non-destructive evaluation of microstructural changes with aging, tempering, creep or service exposure in power generation steels, there are no reports on assessment of the effects of composition differences in the as-service entry or early life material on magnetic signals and, hence, the ability to distinguish between different composition materials in service (in early life condition). The present paper has studied EM sensor responses to P91 steels with different N/Al ratios after a range of selected short term tempering conditions and also after long term aging. The work has assessed the sensitivity of the EM sensor technique to detecting the microstructural differences due to different N/Al ratios and, therefore, the feasibility of sorting out P91 steels of low N/Al ratios.

Materials and experimental details

Sets of samples (measuring ~45 × 40 mm in cross-section and >15 mm in thickness) of three P91 steels of different compositions were supplied by the EPRI in the short term tempered (at a range of temperatures between 649 and 816°C for 1 or 50 h) or long term aged (at 600 or 650°C for 5000 h or 10 000 h) condition. The compositions of the steels are given in Table 1, and heat treatments are summarised in Table 2. As indicated, the samples were selected with significant differences in the N/Al ratio. However, all samples complied with the P91

Table 1 Compositions of P91 steels/wt-%

	C	Mn	Si	Ni	Cr	Mo	V	Nb	N	Al	N/Al
G11	0·11	0·39	0·19	0·27	8·8	0·91	0·21	0·07	0·043	0·033	1·3
G8	0·13	0·43	0·26	0·28	8·2	1·03	0·23	0·07	0·042	0·009	4·7
J4	0·11	0·4	0·29	0·15	8·5	0·92	0·20	0·07	0·054	0·004	13·5

a G11; *b* G8; *c* J4

1 Images (SEM) for as supplied P91 steels of different compositions

specification requirements when the steels were made. It should be noted that ASME have since reduced the level of allowable Al from 0·04 to 0·02 wt-%.[33] The original heat treatment before the short term tempering was normalising at 1060°C for 1 h and before the long term aging was normalising at the same temperature and time, air cooling and then tempering at 760°C for 2 h.

The EM sensor used in the present paper comprises of an H shaped ferrite core that consists of: two vertical legs of 15 mm length and in between a horizontal bar of 10 mm length, all with a $2·5 \times 2·5$ mm square cross-section; an exciting coil wound around the horizontal bar; and two linked up sensing coils wound around the bottom vertical legs. Electromagnetic sensor measurements were carried out by holding the sensor on top of a test sample with the test ends (i.e. the ends of the vertical legs with sensing coils) facing down and in contact with the sample surface, i.e. the stand-off distance being zero. Eight measurements for each sample were carried out at different positions and sensor orientations and averaged. The samples used all had dimensions large enough to avoid any edge effects (or thickness effects) on the EM measurements. All the test surfaces were finely ground to a roughness of $R_a \approx 0·3$ μm (measured with an SE1700 Surfcorder roughness measurement instrument) to provide a uniform effective stand-off

distance and minimise any possible effects of surface roughness. The sensor was excited by a 3 V alternating current supplied by an impedance/phase analyser (Model S1260) made by Solartron Analytical over a range of frequencies from 10 Hz to 10 kHz. Signals picked up by the sensing coil were recorded and processed by the impedance analyser measuring complex transimpedance Z, from which mutual inductance M was calculated as $M = Z/j\omega$, where ω is the angular frequency and j is the imaginary unit.

Metallographic samples for the long term aged samples were mounted, polished to a 0·25 μm diamond paste finish and etched in Kallings reagent. A JEOL-7000 field emission gun scanning electron microscope was used to characterise the microstructure. Metallographic data including SEM and TEM images, together with quantification of the precipitates resolved, for the three steels normalised at 1066°C for 30 min and then tempered at 760°C for 30 min, and electron backscattered diffraction maps for these steels tempered at 788°C for 1 or 50 h were provided by the EPRI[34] and presented in the present paper; these data are representative of the materials assessed in the present work. No corresponding samples were available for EM sensor tests.

The Vickers hardness values for the long term aged samples were measured by the authors using 30 kg load and averaged over five repeats for each samples, while the values for the short term tempered samples have been provided by the EPRI without standard deviation values.
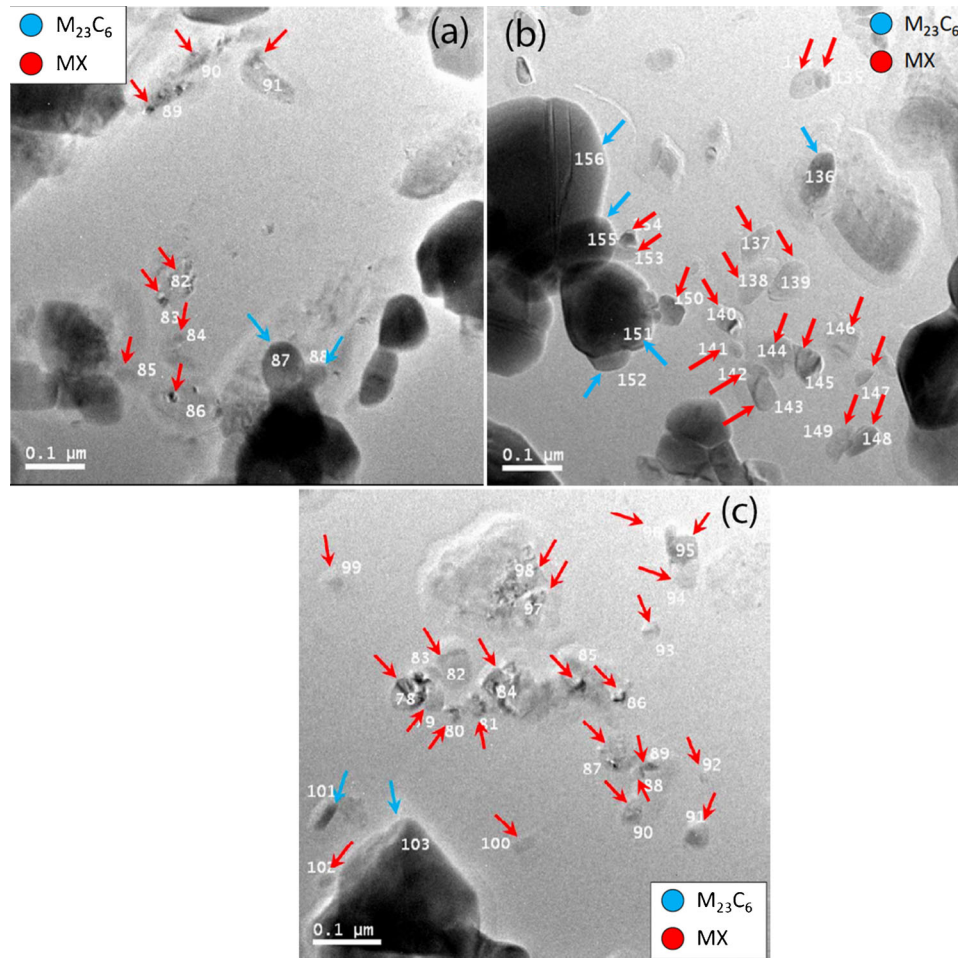
Results

Microstructure

Figure 1 shows the microstructures of the three studied steels with different N/Al ratios in the normalised (1066°C for 30 min) and tempered (760°C for 30 min) conditions. They all show a microstructure of tempered

Table 2 Heat treatment or aging conditions

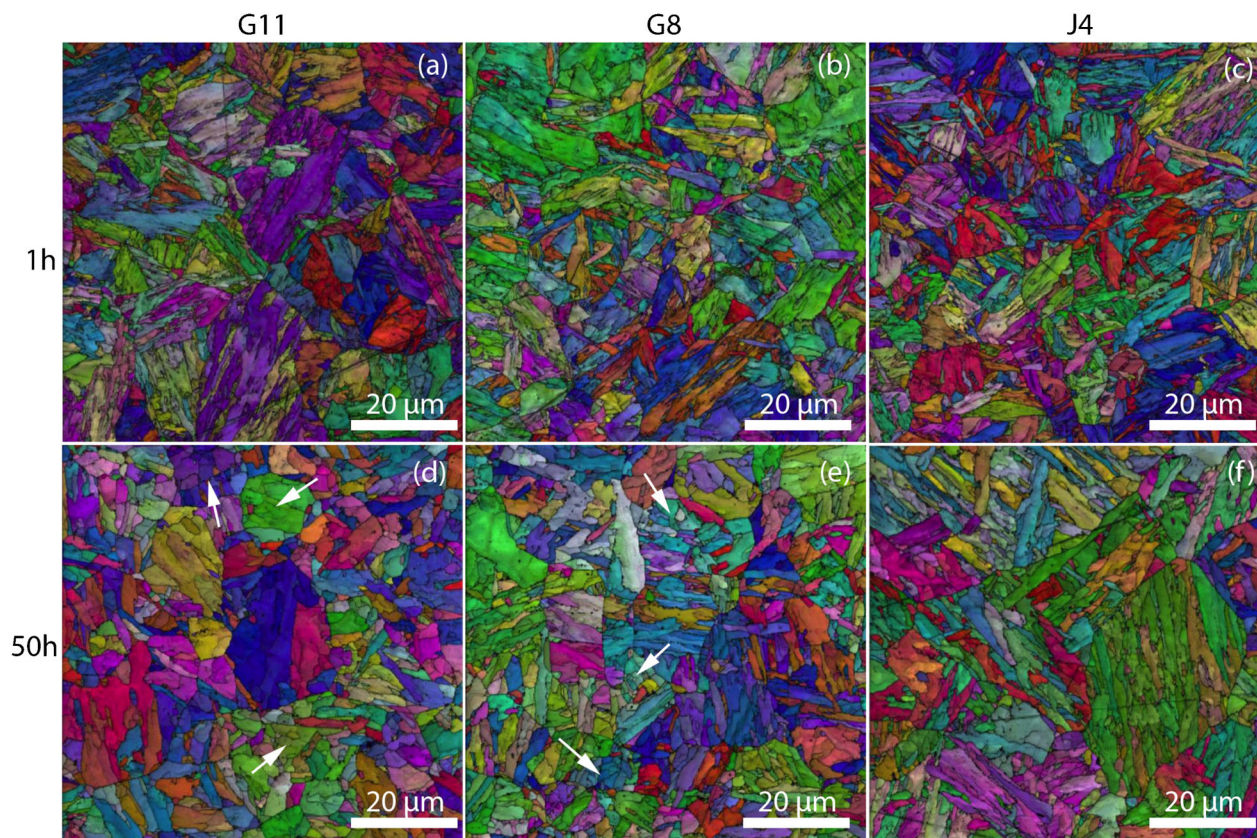| Steel	Sample no. suffix	Heat treatment
G11, G8	S1	Tempering at 649°C for 1 h
	S2	Tempering at 704°C for 1 h
	S3	Tempering at 816°C for 1 h
	S4	Tempering at 774°C for 50 h
G11, G8, J4	L1	Aging at 600°C for 5,000 h
	L2	Aging at 600°C for 10 000 h
	L3	Aging at 650°C for 5000 h
	L4	Aging at 650°C for 10 000 h

a G11; *b* G8; *c* J4

2 Images (TEM) for P91 steels of different N/Al ratios in their service entry condition showing fine intralath precipitates: numbers next to particles in image refer to count of particles analysed[34]

martensite with many carbide precipitates (mostly $M_{23}C_6$)[5,35] present on martensitic lath boundaries. The finer MX precipitates cannot be resolved at these magnifications in the SEM. The major difference between the samples lies in the number density of the fine precipitates occurring within the martensitic laths, which cannot be observed in the SEM images but can be seen clearly in the TEM images for these samples, shown in Fig. 2. There are very few MX precipitates present within the matrix of steel G11 (N/Al≈1·3), while the number density of MX increases significantly in steels G8 and J4 (N/Al>4). Thermo-Calc calculations were carried out for the three compositions for equilibrium at the various heat treatment temperatures (using version S and the TCFe7 database). The predicted volume fraction of the MX precipitates at equilibrium at 760°C (G11, 0·20%; G8, 0·30%; J4, 0·35%) increases with increasing N/Al ratio. There is no significant difference in the size of the MX precipitates between the samples, with the mean equivalent circle diameter measuring between 40 and 50 nm. Therefore, the number densities of the MX precipitates for the steels are expected to increase with the N/Al ratio provided that the MX precipitation is nitrogen limited and the other elements are at similar levels, as confirmed in Table 1. However, it is worth noting that at a high N/Al ratio, e.g. for the J4 sample, where the free nitrogen content is high, the MX precipitation is Nb limited

rather than nitrogen limited, in which case the number density of MX precipitates will reach a maximum value at a N/Al ratio of ~12 as predicted by Thermo-Calc.

Figure 3*a*–*c* shows the electron backscattered diffraction inverse pole figure maps, with an overlay of the relevant grain boundary map, for the three steels tempered at 788°C for 1 h.[34] As the tempering condition is very close to the service entry condition, these microstructures should be representative of the service entry microstructure of the three studied steels. They all show generally similar martensitic lath structures with comparable lath size according to the quantification results given in Table 3. Therefore, based on the microstructural information available, the studied steels with different N/Al ratios in their service entry conditions are expected to consist of tempered martensite, of comparable lath size but with different number densities of intralath MX precipitates as described earlier. The microstructures for the three steels appear to be different after tempering for 50 h at 788°C. The steel G11 (N/Al=1·3) sample has lost much of the lath structure. This change is a consequence of the martensitic structure developing fine equiaxed subgrains, as can be seen in Fig. 3*d*. The steel G8 (N/Al=4·7) sample still largely retains its lath structure with the laths coarsening slightly and some subgrains developing, as shown in Fig. 3*e*, which indicates a slower subgrain development compared to G11. In contrast, there is insignificant lath

3 Electron backscattered diffraction inverse pole figure overlaid with grain boundary maps for three steels tempered at 788°C for 1 (top row) or 50 h (bottom row): white arrows mark some examples of subgrain developing region[34]

coarsening or subgrain development in the steel J4 (N/Al=13·5) sample as can be observed in Fig. 3*f*. These results indicate that the higher the N/Al ratio, the greater the resistance to lath coarsening and/or subgrain development during tempering at high temperature for the studied steels, which can be attributed to the difference in the number density of the fine MX precipitates that plays an important role in pinning mobile dislocations and boundary migration during tempering.[36]

Figure 4 shows the microstructures for the long term aged samples at 650°C for 10 000 h for the three steels. They all have a tempered martensite structure without any significant number of equiaxed subgrains having developed. The less aged samples also have similar microstructures, and therefore, their micrographs are not presented here. The lath widths for all the long term aged samples have been quantified and summarised (mean values with standard deviation) in Table 3. Figure 5 shows the lath width distribution for the long term aged G11 (N/Al=1·3) samples becoming broader as the aging time/temperature increase, which is consistent with the measured mean lath width increasing with the aging time/temperature, as illustrated in Table 3. The lath widths for the long term aged G8 (N/Al=4·7) and J4 (N/Al=13·5) samples, however, remain more or less
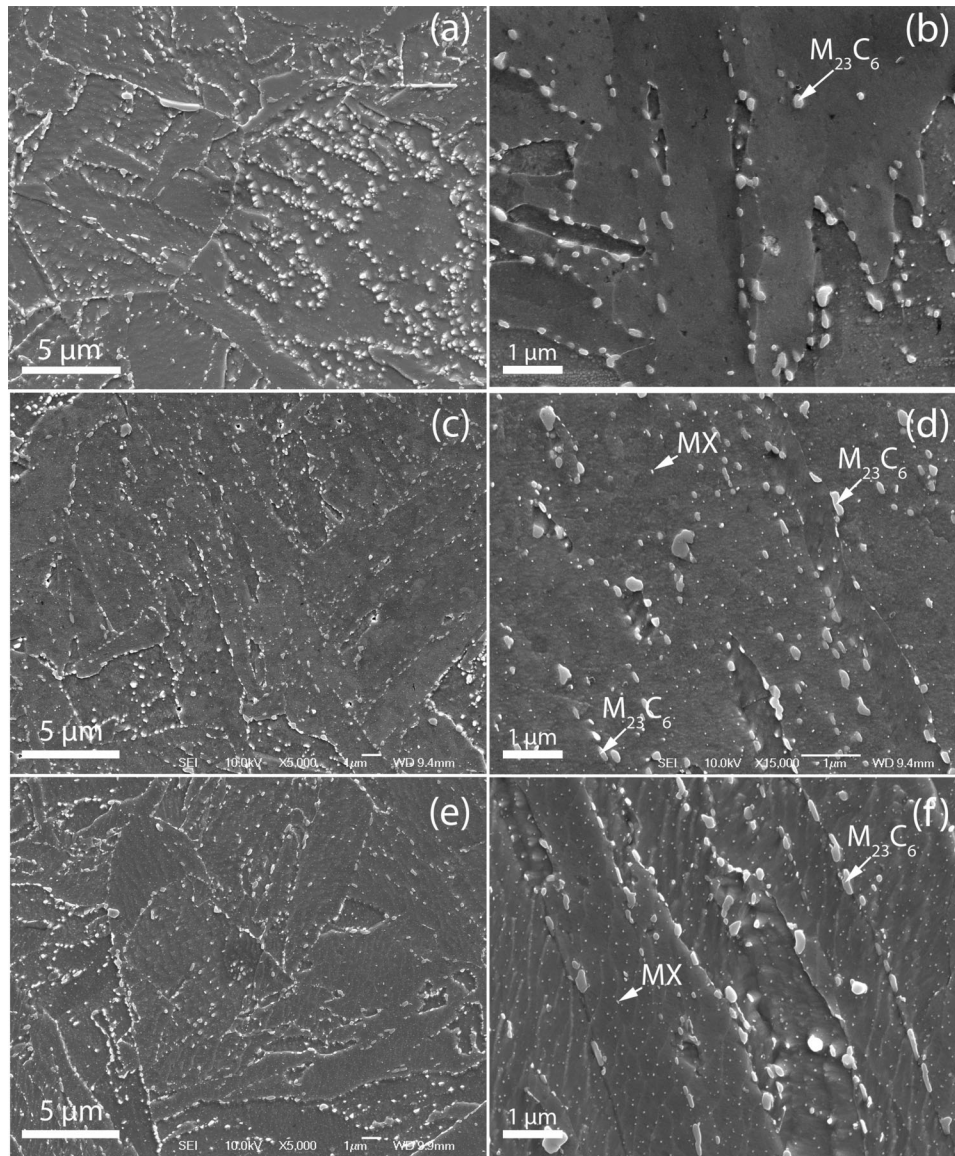
unchanged (Table 3). This indicates that the martensitic lath microstructure in the G8 and the J4 steels change much more slowly than in G11.This difference in behaviour is consistent with the presence of fine intralath MX precipitates, as can be clearly seen in Fig. 4*d* and *f*, pinning mobile dislocations and hence slowing down the aging process. It can also be observed in Fig. 4*b, d* and *f* that the number density of the intralath MX precipitates increases with the N/Al ratio for the three studied steels, which is consistent with the prediction described earlier. Figure 6 compares the lath distribution and corresponding log normal fitting curves for the long term aged samples for the three steels. Although the mode and the mean values of the lath width for the long aged G8 and J4 samples are very close, the latter shows a slightly narrower distribution and a higher probability density for fine laths (0·25–0·75 μm width) than the former. That is, the long term aged J4 samples have slightly finer lath structure than the G8 ones.

Electromagnetic measurements

Figure 7 shows the EM sensor measurements in the form of the real part of the mutual inductance as a function of frequency for the short term tempered samples. The imaginary part of the signal is predomi-
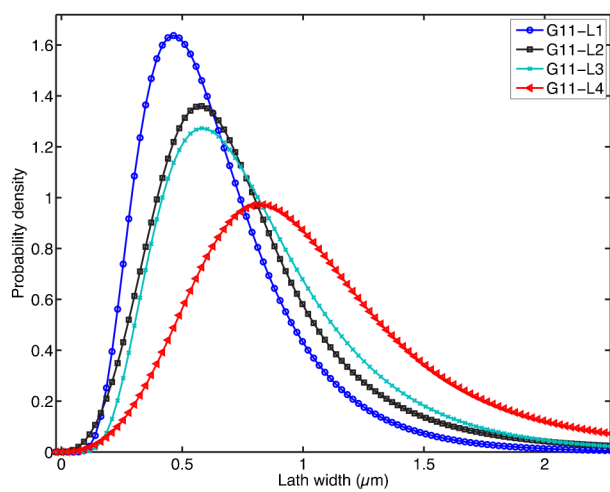
Table 3 Martensitic lath widths for tempered and long term aged samples of three steels/μm

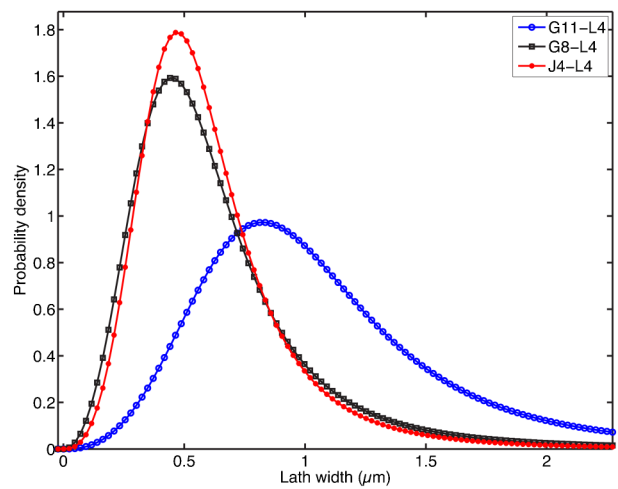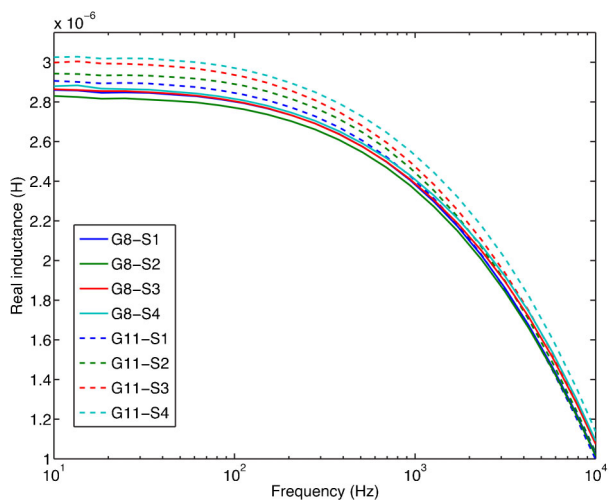|	788°C, 1 h	600°C, 5000 h	600°C, 10 000 h	650°C, 5000 h	650°C, 10 000 h
G11	0·66±0·23	0·66±0·31	0·78±0·41	0·82±0·39	1·07±0·49
G8	0·68±0·26	0·62±0·31	0·67±0·32	0·66±0·32	0·66±0·36
J4	0·63±0·21	0·60±0·30	0·65±0·28	0·63±0·33	0·62±0·31

a, b G11; *c, d* G8; *e, f* J4

4   Images (SEM) for three steels aged at 650°C for 10 000 h: typical examples of $M_{23}C_6$ and MX precipitates are arrowed

5   Lath width distributions and their corresponding log normal fitting curves for long aged G11 samples
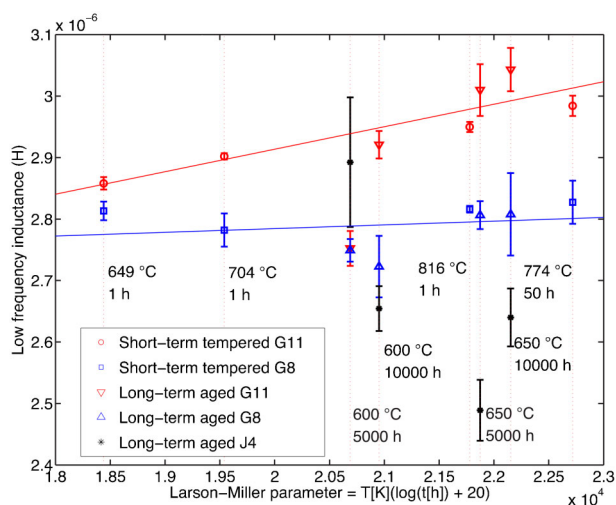

6   Lath width distributions and their corresponding log normal fitting curves for samples aged at 650°C for 10 000 h for three steels
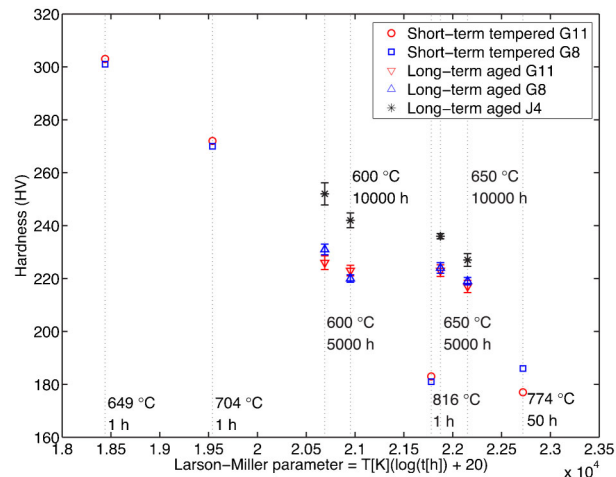
7 Real mutual inductance of sensor coils as function of frequency for short term tempered G8 and G11 samples as identified in Table 2

9 Hardness as function of Larson–Miller parameter for all studied samples

nantly affected by the resistivity of the test samples,[37] which is much less sensitive to the microstructural changes noted in the studied samples[20] and therefore will not be presented in the present paper. The real inductance is essentially independent of frequency over the low frequency (approximately 10–100 Hz) range, where the G11 (N/Al=1·3) and the G8 (N/Al=4·7) set of samples can be clearly distinguished and then drops continuously with increasing frequencies. For conciseness, the inductance value at low frequencies (here taken as the value for 10 Hz) has been used as a characteristic inductance parameter M_0. Over the low frequency range, the relative permeability dominates the M_0 value, as the effects of induced eddy currents are insignificant. As the frequency increases, eddy currents strengthen (and the effect of the material resistivity strengthens accordingly) and reduce the mutual inductance, which accounts for the decreasing (damping) part of real inductance as shown in Fig. 7. Figure 8 plots M_0 as a function of the LMP, a parameter that characterises the amount of thermal exposure incorporating the effects of

both the temperature and duration, for the short term tempered and the long term aged samples. The short term tempered G11 (N/Al=1·3) samples give consistently higher M_0 values than the G8 (N/Al=4·7) samples at similar LMP. It appears that there is an approximately monotonic increase in M_0 with the LMP for the short term aged G11 samples. In contrast, the G8 values remain more or less constant with increasing LMP. Similar trends, that is, the increase in M_0 with the LMP for the G11 set and the G11 values being higher than the G8 ones, have also been observed in the long term aged samples, as shown in Fig. 8. The M_0 values for the long term aged G8 samples appear much less sensitive to the LMP, over the range examined. These trends are illustrated as least square fitted lines in Fig. 8. The J4 (N/Al=13·5) values show much more variability, the reason for which is not clear. However, it can be seen in Fig. 8 that, in general, the higher the N/Al ratio of the studied samples, the lower the M_0 value, particularly after aging at 600°C for 5000 h, which is consistent with the observations made for the short term tempered G8 and G11 samples as shown in Fig. 8.

Hardness

Figure 9 shows the hardness values as a function of the LMP for all the samples. In contrast with the significant difference in M_0 values between the G11 and the G8 samples subjected to the same thermal exposure, the hardness values are similar for the LMPs below 21 780. This indicates that hardness measurement is relatively insensitive to the N/Al ratio for the P91 steels at service entry or early service states where lath/precipitate coarsening is still insignificant. Although they can effectively pin mobile dislocations and improve creep resistance, the intralath MX precipitates play a relatively minor role on hardness, compared to the high angle martensitic block/packet boundaries and the precipitates present on the boundaries (i.e. $M_{23}C_6$), due to their much lower volume fraction.[38,39] At a high LMP, e.g. for tempering at 774°C for 50 h, the hardness values for the G11 and the G8 samples start to differ, which can be ascribed to the development of subgrains reducing the number of boundaries, as can be observed in Fig. 3, and the coarsening of the carbides during tempering at a relatively high temperature being more significant in the

8 Low frequency real inductance M_0 as function of Larson–Miller parameter for short term tempered G8 and G11 samples and long term aged samples for all studied steels

G8 sample. The long aged J4 samples have higher hardness values, which are expected of the finer lath structure as described earlier.

Discussion

It should be noted that the EM sensor measurements at low frequencies, using a small applied magnetic field such as in the present work, are sensitive to the initial relative permeability of the test materials. This has been discussed in our previous paper,[20] which demonstrated that the low frequency inductance M_0 increase with the initial relative permeability exponentially, and the latter is affected by the microstructural features that determine the mean free path for domain wall motion in a small magnetic field. For example, the initial permeability values for P9 and T22 steels in different heat treatment/ex-service conditions, measured by the EM sensors, increase with the mean free path for domain wall motion approximately by a power law at an exponent of −1.[20] It is worth noting that evaluating relative permeability and resistivity from the present H shaped EM sensor measurements of the block samples, by fitting the test data with finite element modelled inductance, is not impossible, but the computational cost would be high as a three-dimensional model is required for the H shaped EM sensor, compared to the two-dimensional axisymmetric model for a cylindrical system (using a cylindrical sample and a cylindrical sensor) as presented previously elsewhere.[20] However, no cylindrical samples of these materials were available, and the provider did not permit machining of the original samples. These tests may be carried out in the future to establish a more robust, quantitative relationship between composition changes within the P91 specification and EM signals or relative permeability of the steels, which might also address the variability issues seen for the J4 samples.

For tempered martensitic microstructures without any significant numbers of intralath precipitates, such as all the G11 samples, the martensitic lath boundaries are the effective pinning sites to domain wall movement. The intralath dislocations are of low density and are expected to cause insignificant disturbance to domain walls.[40] The $M_{23}C_6$ precipitates occurring mostly on the lath boundaries play a relatively minor role in pinning domain walls, as the grain/lath boundaries are the major pinning features in this case.[20] Therefore, the mean free path for domain wall motion, and hence the relative initial permeability, is governed by lath width. Accordingly, the monotonic increase in the M_0 values of the short term tempered or the long term aged G11 samples with the LMP can be attributed to coarsening of the martensitic laths during thermal exposure, as shown in Fig. 3 for the short term aged conditions and as reported[41,42] on similar modified 9Cr–1Mo steels showing lath coarsening after a comparable amount of thermal exposure, increasing the mean free path for domain wall motion and hence the initial permeability.

For the tempered martensite microstructures with a significant number of precipitates present within the laths, such as the G8 and the J4 samples, the lath boundaries will still act as pinning sites to domain walls. However, the intralath precipitates may also influence the mean free path for domain wall motion. It has been reported that effective pinning sites typically have linear dimensions of 5–100 nm (Ref. 43), and inclusions are mostly effective in pinning domain walls when their size

is equivalent to the domain wall thickness.[44] The size of the MX precipitates in the present study (about 40–50 nm in equivalent circle diameter) is within the range for effective size and expected to be in the same order of the domain wall thickness (reported to be ~39 nm for pure iron).[45] In addition, they are non-magnetic particles containing no Co or Ni and a negligible amount of Fe (three orders of magnitude lower in mass fraction than Nb and V according to Thermo-Calc modelling). These particles have a face centred cubic structure; therefore, there will be free magnetic poles present around them, which can generate a significant disturbance to the domain wall energy when the domain walls intercept with them according to Neel's theory.[46] Therefore, the intralath MX precipitates are expected to be effective in pinning domain walls in a small magnetic field. It follows that their interparticle spacing, or number density as a first approximation to a uniform distribution, determines the mean free path for domain wall motion. The higher the number density, the shorter the mean free path for domain wall motion and hence the higher the initial relative permeability expected. Accordingly, it can be expected that the number density of MX precipitates within the laths will increase with an increase in the N/Al ratio (for all other compositional factors remaining constant) reducing the mean free path for domain wall motion and hence the initial relative permeability. Therefore, it is expected that the higher the N/Al ratio in the studied P91 steels, the lower the M_0 value will be for a given LMP. Coarsening of the MX precipitates is expected to be insignificant for the thermal exposure that the short term tempered G8 samples have been through according to,[5,35] or for the long term aged G8 and J4 samples, as can be observed in Fig. 4. These fine MX particles also enhance the microstructural stability to lath coarsening during the thermal exposure. Thus, the reduced sensitivity of the M_0 values to the LMP for the G8 and J4 samples compared to the G11 samples is expected due to the stability of the intralath MX precipitates, the reduced rate of lath coarsening and hence the insignificant changes to the mean free path for domain wall motion and the initial relative permeability.

Sensitivity to intralath MX precipitates enables the present EM sensor to differentiate P91 steels with different N/Al ratios non-destructively, particularly when the steels are in the service entry or early service condition. Nevertheless, it should be noted that the sensitivity relies on the intralath precipitates effectively pinning domain walls and influencing the mean free path for domain wall motion during the EM sensor tests. That is, their pinning strength to domain walls must be greater than the critical pinning strength that the domain walls can overcome under the influence of the measurement magnetic field. If a strong magnetic field is applied during EM sensor tests, for example by applying a strong bias field or using a large sensor with a larger driving current, it is possible that the domain walls will overcome the pinning from the fine intralath MX precipitates. In such cases, the EM sensor is not expected to be sensitive to the intralath MX precipitates but to the pinning features that can effectively pin the domain walls.

The present laboratory based EM sensor may be scaled up for industrial deployment for sorting out the P91 steel components of low N/Al ratio before they enter service, with dedicated sensor design. A large

sensor is expected to reduce the scatter that is usually suffered by small sensors and caused by operational factors, e.g. sensor angling or stand-off distance variability or local microstructural variability (e.g. due to macroscale segregation or local accidental exposure to high temperature). Results from a prototype deployable sensor measuring misheat treated and short term aged 53 mm outside diameter tube samples is given elsewhere.[47] Ambient magnetic field, usually unknown and complex especially in industrial applications, or the variability of the impedance analyser driving the sensor can also cause scatter, which can be eliminated or reduced by employing dummy sensing coils (measuring the air) together with the active ones (measuring the sample) with a common exciting coil as described in detail elsewhere.[27] Thus, the sensitivity to material effects can be improved. Calibration of the sensor for a range of N/Al ratios below 4 is needed to determine the threshold value of the EM signal, e.g. the low frequency inductance and the required accuracy.

Conclusions

The present EM sensor is capable of separating P91 steels with low N/Al ratios in the short term tempered or long term aged condition, based on the principle that the N/Al ratio significantly affects the number density of the intralath MX carbonitride precipitates. These precipitates determine the mean free path to domain wall motion and hence the initial relative permeability of the steels and the measured low frequency inductance M_0 values. In contrast, hardness measurements were found to be insensitive to the N/Al ratio for the short term tempered samples.

Acknowledgements

References

1. M. E. Abd El-Azim, O. E. El-Desoky, H. Ruoff, F. Kauffmann and E. Roos: *Mater. Sci. Technol.*, 2013, **29**, (9), 1027–1033.
2. R. A. Barrett, T. P. Farragher, N. P. O'Dowd, P. E. O'Donoghue and S. B. Leen: *Mater. Sci. Technol.*, 2014, **30**, (1), 67–74.
3. A. Fujio: *Sci. Technol. Adv. Mater.*, 2008, **9**, (1), 013002.
4. B. Shashank Dutt, M. Nani Babu, S. Venugopal, G. Sasikala and A. K. Bhaduri: *Mater. Sci. Technol.*, 2011, **27**, (10), 1527–1533.
5. Å. Gustafson and M. Hättestrand: *Mater. Sci. Eng. A*, 2002, **A333**, (1–2), 279–286.
6. S. Spigarelli, E. Cerri, P. Bianchi and E. Evangelista: *Mater. Sci. Technol.*, 1999, **15**, (12), 1433–1440.
7. S. J. Brett, J. S. Bates and R. C. Thomson: 'Aluminium nitride precipitation in low strength grade 91 power plant steels', Proc. 4th Int. Conf. on 'Advances in materials technology for fossil power plants', Materials Park, OH, USA, June 2005, ASM International, 1183–1197.
8. S. J. Brett: 'Service experience with a retrofit modified 9Cr (grade 91) steel header', Proc. 5th Int. Conf. on 'Advances in materials technology for fossil power plants', Marco Island, Florida, March 2008, ASM International, 590–600.
9. J. Parker and S. Brett: *Int. J. Pres. Ves. Pip.*, 2013, **111–112**, 82–83.
10. J. Parker: 'Best practice guideline for manufacturing and construction of grade 91 steel components', 1023199, Electric Power Research Institute, Palo Alto, CA, USA, 2011.
11. EPRI: 'Review of weld repair options for grade 91. Part 2: damage development and distribution', 3002000087, EPRI, Palo Alto, CA, USA, 2013.
12. D. Jiles: 'Introduction to magnetism and magnetic materials'; 1998, London, Chapman and Hall.
13. D. J. Buttle, G. A. D. Briggs, J. P. Jakubovics, E. A. Little, C. B. Scruby, G. Busse, C. M. Sayers and R. E. Green: *Philos. Trans. R. Soc. A*, 1986, **320A**, (1554), 363–378.
14. J. N. Mohapatra, J. Swaminathan, M. K. Ghosh and A. Mitra: *Metall. Mater. Trans. A*, 2010, **41A**, (4), 900–905.
15. A. Mitra, J. N. Mohapatra, J. Swaminathan, M. Ghosh, A. K. Panda and R. N. Ghosh: *Scr. Mater.*, 2007, **57**, (9), 813–816.
16. H. Kumar, J. N. Mohapatra, R. K. Roy, R. Justin Josephus and A. Mitra: *J. Mater. Process. Technol.*, 2010, **210**, (4), 669–674.
17. C. J. Bong, K. S. Ryu, S. H. Nahm and E. K. Kim: *J. Magn. Magn. Mater.*, 2011, **323**, (5), 379–382.
18. V. Moorthy, S. Vaidyanathan, T. Jayakumar and B. Raj: *Philos. Mag. A*, 1998, **77A**, (6), 1499–1514.
19. W. Yin, X. J. Hao, A. J. Peyton, M. Strangwood and C. L. Davis: *NDT&E Int.*, 2009, **42**, (1), 64–68.
20. J. Liu, M. Strangwood, C. Davis and A. Peyton: *Metall. Mater. Trans. A*, 2013, **44A**, (13), 5897–5909.
21. L. Zhou, J. Liu, X. J. Hao, M. Strangwood, A. J. Peyton and C. L. Davis: *NDT&E Int.*, 2014, **67**, 31–35.
22. U. Bohnenkamp, R. Sandstrom and G. Grimvall: *J. Appl. Phys.*, 2002, **92**, (8), 4402–4407.
23. U. Bohnenkamp and R. Sandstr: *Steel Res.*, 2000, **71**, (10), 410–416.
24. D. Ludwigson and F. Schwerer: *Metall. Mater. Trans. B*, 1971, **2B**, (12), 3500–3501.
25. J. W. Byeon and S. I. Kwun: *Mater. Trans.*, 2003, **44**, (6), 1204–1208.
26. U. B. Baek, Y.-H. Lee, H. J. Na, S. H. Nahm and Y. H. Nam: *Int. J. Mod. Phys. B*, 2010, **24B**, (15n16), 2441–2446.
27. S. J. Dickinson, R. Binns, W. Yin, C. Davis and A. J. Peyton: *IEEE Trans. Instrum. Meas.*, 2007, **56**, (3), 879–886.
28. W. Zhu, H. Yang, A. Luinenburg, F. van den Berg, S. Dickinson, W. Yin and A. J. Peyton: *Ironmak. Steelmak.*, 2014, **41**, (9), 685–693.
29. X. Hao, W. Yin, M. Strangwood, A. Peyton, P. Morris and C. Davis: *Metall. Mater. Trans. A*, 2009, **40A**, (4), 745–756.
30. X. Hao, W. Yin, M. Strangwood, A. Peyton, P. Morris and C. Davis: *Scr. Mater*, 2008, **58**, (11), 1033–1036.
31. R. J. Haldane, W. Yin, M. Strangwood, A. J. Peyton and C. L. Davis: *Scr. Mater.*, 2006, **54**, (10), 1761–1765.
32. J. Liu, X. J. Hao, L. Zhou, M. Strangwood, C. L. Davis and A. J. Peyton: *Scr. Mater.*, 2012, **66**, (6), 367–370.
33. ASTM: 'Standard specification for seamless ferritic alloy-steel pipe for high-temperature service', A335/A335M-09a, ASTM International, West Conshohocken, PA, USA, 2009.
34. EPRI: 'Life management of creep strength enhanced grade 91 steel – atlas of microstructure', 3002000080, Electric Power Research Institute, Palo Alto, CA, USA, 2013.
35. C. G. Panait, A. Zielinska-Lipiec, T. Koziel, A. Czyrska-Filemonowicz, A.-F. Gourgues-Lorenzon and W. Bendick: *Mater. Sci. Eng. A*, 2010, **A527**, (16–17), 4062–4069.
36. F. Abe, T. Horiuchi, M. Taneike and K. Sawada: *Mater. Sci. Eng. A*, 2004, **A378**, (1–2), 299–303.
37. N. Karimian, J. W. Wilson, A. J. Peyton, W. Yin, J. Liu and C. L. Davis: *J. Magn. Magn. Mater.*, 2014, **352**, (0), 81–90.
38. H. Hirukawa, S. Matsuoka, K. Miyahara and Y. Furuya: *Mater. Lett.*, 2004, **58**, (3–4), 321–325.
39. K. Sawada, K. Miyahara, H. Kushima, K. Kimura and S. Matsuoka: *ISIJ Int.*, 2005, **45**, (12), 1934–1939.
40. B. Astie, J. Degauque, J. L. Porteseil and R. Vergne: *IEEE Trans. Magn.*, 1981, **17**, (6), 2929–2931.
41. P. J. Ennis, A. Zieliska-Lipiec and A. Czyrska-Filemonowicz: *Mater. Sci. Technol.*, 2000, **16**, 1226–1233.
42. K. Sawada, K. Kubo and F. Abe: *Mater. Sci. Technol.*, 2003, **19**, (6), 732–738.
43. P. Gaunt: *Can. J. Phys.*, 1987, **65**, (10), 1194–1199.
44. C. S. Kim, C. J. Lissenden, I. K. Park and K. S. Ryu: *Mater. Trans.*, 2009, **50**, (11), 2691–2694.
45. D. Jiles: 'Domain walls', in 'Introduction to magnetism and magnetic materials', (ed. D. Jiles), 171–175; 1998, London/New York, Chapman and Hall/CRC.
46. L. Neel: *Cah. Phys.*, 1944, **25**, 21–44.
47. J. W. Wilson, J. Liu, N. Karimian, C. L. Davis and A. J. Peyton: 'Assessment of microstructural changes in grade 91 power station tubes through permeability and magnetic Barkhausen noise measurements', Proc. European Conf. on 'Non-destructive testing', Prague, Czech Republic, October 2014.